FULL PAPER

18.45%-Efficient Multi-Crystalline Silicon Solar Cells with Novel Nanoscale Pseudo-Pyramid Texture

*Xiaoya Ye, Shuai Zou, Kexun Chen, Jianjiang Li, Jie Huang, Fang Cao, Xusheng Wang, Lingjun Zhang, Xue-Feng Wang, Mingrong Shen, and Xiaodong Su**

Silicon-based cells could convert more solar energy to electrical energy if the cells could absorb more light. However, the nanostructured cells have demonstrated relatively low power conversion efficiency even when its reflection is very low; thus, they are still far from becoming real products of the photovoltaic industry. Here, nanoscale pseudo-pyramid textured multi-crystalline silicon (Pmc-Si) solar cells, with the best efficiency of ≈18.45%, are fabricated by using a metal-catalyzed chemical etching plus a post alkaline etching on an industrial production line. Such Pmc-Si solar cells have showed similar light trapping ability as single crystalline silicon solar cells of micrometer pyramid texture, and the improved efficiency is mainly ascribed to its enhanced light absorption while the nanostructured surface still keeps acceptable passivation quality, that is, the short-circuit current density has an increase of ≈300 mA cell^{-1}, while the open-circuit voltage has only a slight decrease of ≈1 mV. Further elevations of the efficiency are expected by optimizing both micrometer- and nanotextures, and exploring more effective passivation technique. More excitingly, the technique presented here has been verified in the production line for several batches as a real technique of low cost and high efficiency.

1. Introduction

In the past decade, the power conversion efficiency η of single crystalline silicon (*sc*-Si) and multi-crystalline silicon (*mc*-Si) solar cells has shown about 0.5% improvement each year, and now it is over 19% for *sc*-Si and over 17% for *mc*-Si in most industrial production lines.[1] As a planar *p-n* junction-based optoelectronic device, the η of Si solar cells has been elevated from two aspects: one is the electrical properties, i.e., the quality of Si wafer, surface passivation, selective emitter, back surface field, etc;[2,3] and the other is the optical properties to reduce light losses, i.e., the front texture and antireflection coating, the interdigitated back contact solar cells, metal wrap through solar cell, etc.[4,5]

Although *mc*-Si solar cells have occupied more than 70% of the photovoltaic (PV) market, the η of *mc*-Si solar cells is still about 2% lower than that of *sc*-Si cells, due to not only its large number of grain boundaries, which act as recombination centers of electron–hole (*e-h*) pairs, but also its poor ability for trapping light at the front textured surface. It is well accepted that a pyramid texture can be formed on *sc*-Si wafer based on anisotropic alkali etching, but is not applicable to the *mc*-Si.[6] Alternatively, random pits or a honeycomb texture are formed on the surface of *mc*-Si based on isotropic acidic etching.[7] Together with anti-reflection coating (ARC) and surface texture, the *sc*-Si shows a lower average reflectivity $\overline{R}$ (ca. 5%, in a wavelength range from 350 to 1050 nm) compared to that of *mc*-Si (ca. 12%). Therefore, it gives a potential space to raise η, even breaking 18%, if more effective light-trapping texture can be fabricated into *mc*-Si cells.

Recently, nanostructure textured black silicon with extremely low reflectivity (near to zero) has attracted intensive attention due to its great potential for applications in silicon-based solar cells.[8–10] There are several advantages of black silicon solar cells: the excellent light-trapping over a wide spectrum range from 300–2000 nm;[11] the possibility of removing the expensive vacuum processing of plasma-enhanced-chemical-vapor-deposition (PECVD); and the wider acceptance angle of light.[12] Mainly, there are three kinds of techniques to fabricate black silicon: laser texturing,[8,13] reactive ion etching (RIE),[10,14,15] and metal-catalyzed chemical etching (MCCE).[9,16–18] For industrial production, the RIE and MCCE techniques have obtained high expectations, but obviously MCCE is much more suitable for the current production line, where the conventional texturing process is also based on wet chemical etching. Oh et al. reported an 18.2% efficiency in black single-crystalline silicon (B*sc*-Si) solar cells.[19] Although the efficiency is still lower than that of industry level, it demonstrates a great progress in MCCE technique. However, the reported efficiencies for black multi-crystalline silicon (Bmc-Si) solar cells based on either RIE or MCCE are still very low, i.e., 12–16.6%. **Table 1**

X. Ye, S. Zou, K. Chen, J. Li, J. Huang, F. Cao, Dr. X. Wang, Dr. L. Zhang, Prof. X.-F. Wang, Prof. M. Shen, Prof. X. Su
College of Physics, Optoelectronics and Energy
Collaborative Innovation Center of Suzhou Nano Science and Technology
Photovoltaic Research Institute of Soochow University & Canadian Solar Inc.
and Jiangsu Key Laboratory of Thin Films
Soochow University
1 Shizi street, Suzhou 215006, PR China
E-mail: xdsu@suda.edu.cn

DOI: 10.1002/adfm.201401589

Table 1. State-of-the-art nanostructured Si solar cells.

Cell (type, size)	Method	Passivation and ARC	R [%]	η [%]
mc-Si (P, 15.6 cm × 15.6 cm)	RIE	PECVD-SiN_x	13.7	16.1[10]
mc-Si (P,15 cm × 15 cm)	RIE	PECVD-SiN_x	N/A	17.1[21]
sc-Si (N, 4 cm^2)	RIE	ALD-Al_2O_3	1.9	18.7[22]
sc-Si (P, 0.8081 cm^2)	MCCE ($AgNO_3$)	Thermal oxide SiO_2	4.6	18.2[19]
sc-Si (P, N/A)	MCCE ($AgNO_3$)	Al_2O_3	2.5	18.2[23]
mc-Si (P, 4 cm^2)	MCCE ($AgClO_4$)	PECVD-SiN_x	22	16.6[24]

lists the state-of-the-art of black Si solar cells. The presented techniques are still at the laboratory- rather than industry-scale. Certainly, the nanostructured silicon can absorb sunlight over a broad range of wavelengths and incidence angle, but it also introduces more recombination centers and nonuniform doping into cell.[19,20] Therefore, a tradeoff between optical gain and recombination loss must be considered to achieve high efficiency.

In this work, we report that a novel nano-scale pseudo-pyramid texture can be formed on the surface of *mc*-Si wafer by using an MCCE technique plus an additional alkaline etching. An efficiency of ca. 18.45% has been achieved in the industry production line of Canada Solar Inc. @ Suzhou.

2. Approach and Mechanism to Nanoscale Pseudo-Pyramid Textured *mc*-Si Wafer

Figure 1a is an illustration of three main steps in preparing a nanoscale pseudo-pyramid texture on the acid-etched *mc*-Si wafer. Figure 1b is an SEM image of the silicon wafer surface

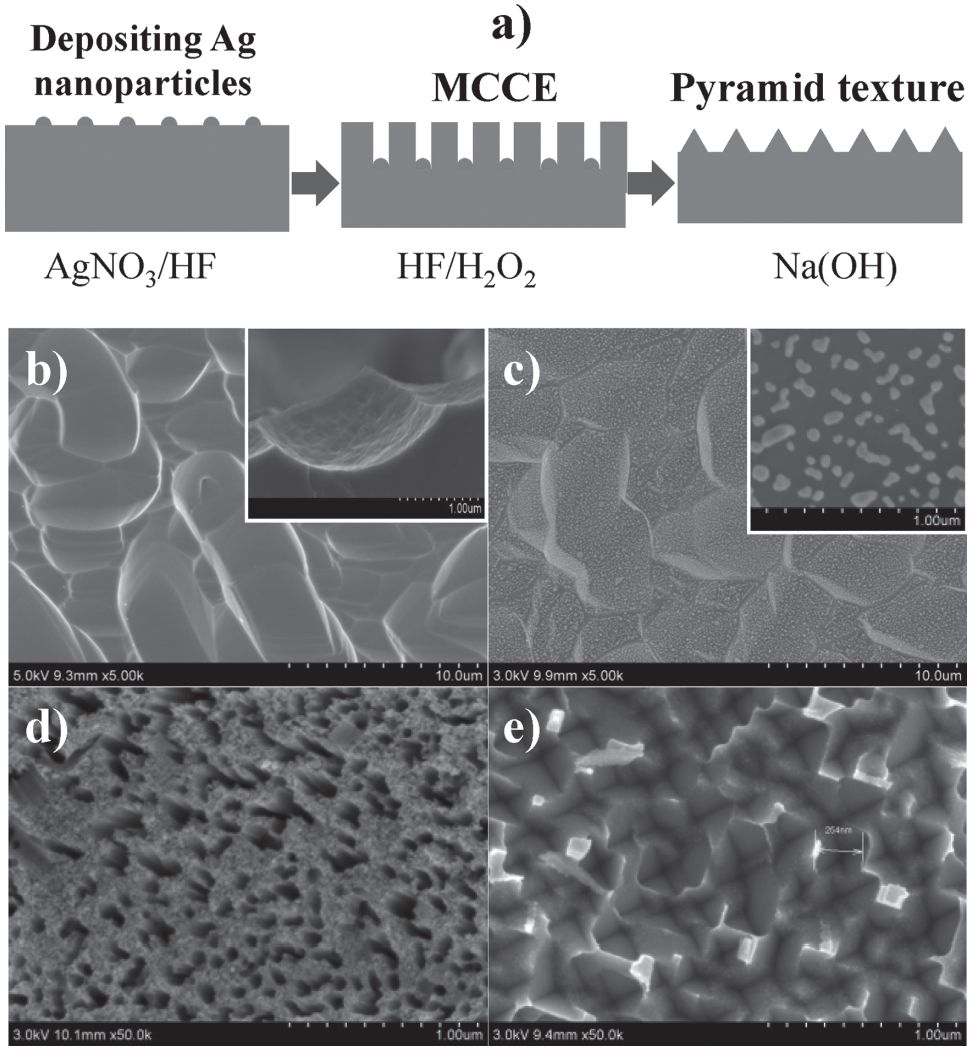

Figure 1. a) Schematic illustration of three main steps preparing nanoscale pseudo-pyramid texture, and SEM surface images of silicon wafer, b) HNO_3/HF acid etching to obtain a typical micrometer texture, inset: the cross-section of the wafer, c) dipping in $AgNO_3$/HF solution to form Ag nanoparticles, inset: large magnification showing the distribution of Ag nanoparticles, d) Ag-catalyzed chemical etching in HF/H_2O_2 and the nanohole texture obtained as the Ag nanoparticles dig into the wafer, and, e) post-etching in Na(OH) solution to convert nanohole texture into nanoscale pseudo-pyramid texture.

after a normal acid texture process in the production line. Homogeneously distributed oval pits have an opening size of about several micrometers, and a depth of about several hundred nanometers (as shown in the insert of Figure 1b). We use the micrometer-textured *mc*-Si wafer as a substrate for the growth of Ag nanoparticles by simply dipping it in the $AgNO_3$/HF mixture solution for 10 s. In this step, the Ag ions inject holes into the valence band of the Si substrate, and then are reduced and form nuclei on the surface of the Si; in parallel, holes injected into the Si substrate oxidize the Si to Si oxide.[25] Figure 1c shows that Ag nanoparticles of a diameter about 20–50 nm have formed on the wafer dispersedly, and have covered ca. 28% of the total area of the wafer. It has been reported that the dendrite structures of silver can be formed on the Si substrate for a relatively long time (e.g., longer than 30 min);[26] in our case, about 10 s deposition can result in some irregular congestion of silver particles, as a close observation from the insert of Figure 1c.

During the etching of the Ag-loaded silicon wafers in HF and H_2O_2 mixture solution, there are two main parameters determining the resulted microstructures: one is the shape of the Ag nanoparticles; another is the ratio of etchant and oxidant. Defining a parameter ρ as the molar ratio of [HF]/([HF] + [H_2O_2]), we have $\rho = 96.3\%$ for our refined solution. It has been suggested that the etching rate is almost completely determined by the concentration of H_2O_2 for a high percentage of HF ($100\% > \rho > 70\%$), which results in nearly all holes generated at the Ag/Si interface.[27] The morphology shown in Figure 1d is in consistent with the above conclusions. With the increase of etching time, the local silicon area under Ag nanoparticles is etched faster than the naked silicon area, and the Ag nanoparticles sink at the bottom of nanopores;[28] meanwhile, the nanoholes become larger gradually and thus connect to each other. After 2 min etching in HF/ H_2O_2, the diameter of nanoholes becomes ca. 20–50 nm, almost equal to that of Ag nanoparticles, and their depth is ca. 350 nm.

We have made the B*mc*-Si solar cells from nanohole-textured wafers of very low reflectivity, around 2–5%, after HNO_3 dipping and a standard SC2 cleaning process to remove the Ag particles, but their efficiencies are in a range of 13–16.5%, which is significantly lower than that 17.5% in normal *mc*-Si solar cells. A well-accepted reason for the low η is that the number of recombination centers which is proportional to the high surface area of the nanostructure has increased largely.[19,29] Besides, we believe that the Ag nanoparticles inside the deep nanostructure are difficult to remove completely even after both HNO_3 and SC2 cleaning processes.

Therefore, the nanohole-textured wafer should be refined in aim to reduce the surface area of wafer and facilitate removal of residual Ag nanoparticles. It was reported that NaOH solution can convert a microporous Si layer into an inverted-pyramid one effectively.[24,30] In our case, by careful etching of the nanohole textured wafer in a Na(OH) based solution, a nanoscale pseudo-pyramid textured mc-Si wafer (P*mc*-Si) can be obtained, as shown in Figure 1e. The average height of the pseudo-pyramids is about 150 nm, which is much lower than the depth of nanohole (ca. 350 nm). In this work, three *mc*-Si wafers/cells (i.e., *mc*-Si, B*mc*-Si. and P*mc*-Si) of different textures have been investigated with respect to their microstructure, optical and PV properties, etc.

The *mc*-Si wafer consists of a lot of millimeter-sized single crystals of various grain orientations, and can also form the micrometer-sized pyramid textures under an anisotropic alkali etching. However, the normal of pyramids (<100>) and etching rate of indivual single crystal depend on its oritentation, resulting in remarkably different microstuctures between *mc*-Si and *sc*-Si wafers (see Supporting Information S1).[31] Fortunately, the above results have shown that the nanosized pseudo-pyramid texture can be formed on the surface of *mc*-Si wafers. It is worth studying how such texture was devoloped from the nanopores. In this work, three kinds of etching process have been applied to the *mc*-Si wafers: the first is the isotropic acid etching to remove the saw-damage and form the micrometer texture; the second is the anisotropic MCCE to form nanopores in the micrometer textures; the third is the anisotropic alkaline etching to transfer nanopores into nanopyramids, which can be explained by the back-bond breaking theory.[32,33] To clarify the etching mechanism of nanopyramids in *mc*-Si, it is helpful to control the surface microstructure of solar cells. The formation mechanism of pseudo-pyramids for *mc*-Si will be discussed next.

The TEM image of the nanoholes in B*mc*-Si sample, as shown in **Figure 2**a, confirmed that the nanoholes are <100> oriented dominantly no matter the sample position. In our case, with $\rho \approx 96.3\%$, the digging direction of Ag nanoparticles is along the crystallographically preferred <100> direction,[34] which is mainly driven by the oxidation rate.[35] Consequently, <100> oriented nanoholes are formed in the surface of micrometer-textured *mc*-Si wafer, and its depth can be easily controlled by etching time. Putting such wafer into Na(OH) solution, some silicon pillars of irregular shape emerged in 60 s as the nanoholes become larger and interconnected (see Supporting Information S2). Note that, each silicon pillar, as a nanosized single crystal, is expected to have an anisotropic etching in Na(OH) solution. In very short time (2–3 mins), those nanopillars can be converted into nanosized pyramids, as shown in Figure 2b. This confirms that the alkaline etching process leads to the formation of {111} pyramidal structures on the silicon surface, and such geometry allows that the light can be more easily coupled into the silicon and efficiently absorbed into the solar cell. Figure 2c schematically presents the formation a nanopyramid from a nanopillar, where the surface area of P*mc*-Si wafer is reduced largely (see Supporting Information S3).

3. Passivation and Antireflection of Nanostructured *mc*-Si Wafer

In a solar cell, the short wavelength photons (350–600 nm) are absorbed in a very thin layer of the surface, where the light-generated *e-h* pairs in the nanostuctured area will be easily recombined at a poorly passivated surface instead of reaching and being separated in the *p-n* junction. The situation is worse in B*mc*-Si solar cells than that in normal *mc*-Si solar cells due to not only a high surface area but also high doping concentration in the emitter.[19] It is expected that the P*mc*-Si wafer has better passivation than B*mc*-Si one due to the shallower and opener nanostructure. Nevertheless, a SiN_x is still necessary for both passivation and antireflection in our samples.[30]

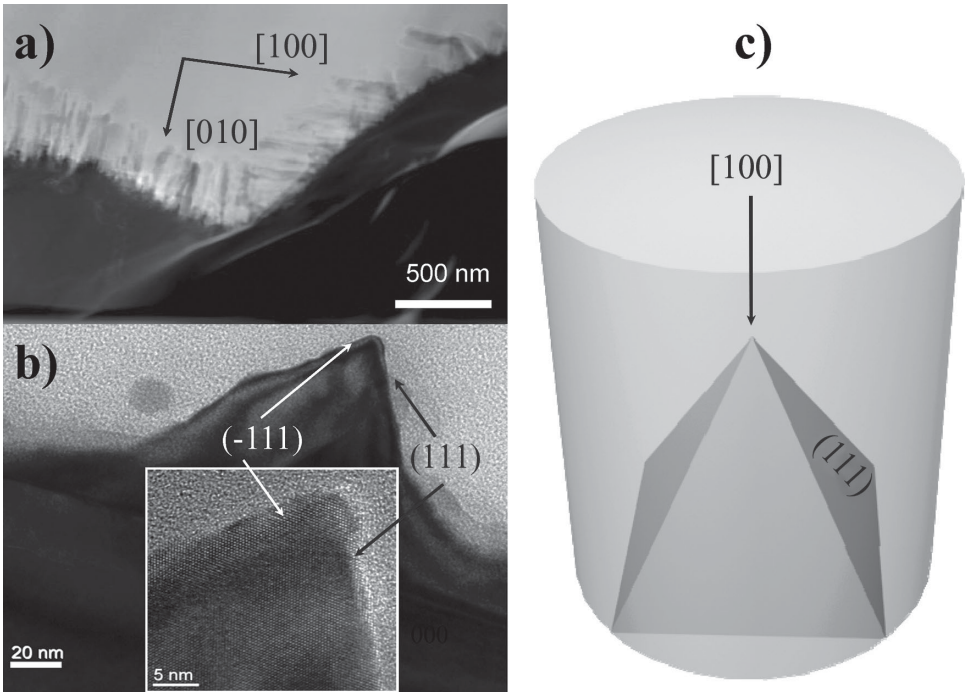

Figure 2. TEM cross-sectional images: a) nanohole textured B*mc*-Si, where the nanoholes are <100> oriented dominantly, b) pseudo-pyramid-textured P*mc*-Si, insert: high resolution image of a typical pyramid featured as two (111) faces; and, c) schematic presentation of the formation of a nanoscale pseudo-pyramid from a nanopillar.

Figure 3 shows the surface and cross-sectional SEM images of SiN_x on the wafers of different textures. Obviously, SiN_x is totally conformal to the micrometer-textured surface of *mc*-Si, and is almost conformal to the pseudo-pyramid textured surface of P*mc*-Si, but SiN_x seems piled up on the top of the nanopore-textured B*mc*-Si. This implies that the thickness and shape of the SiN_x layer depends strongly on the opening and depth of microstructure. Certainly, the SiN_x is difficult to completely cover all of those nanopores of a depth about 350 nm and to fulfill an effective passivation, thus resulting in bad performance in terms of efficiency. A more effective passivation technique must be explored for the highly nanostructured solar cells. Based on the thickness of the conformal SiN_x layer (the same amount of SiN_x mass/volume is assumed to deposit on the projecting area of wafer in PECVD process.), i.e., 91.3 nm for *mc*-Si, and 63.5 nm for P*mc*-Si, we can calculate roughly that the surface area of P*mc*-Si is about 1.44 times of *mc*-Si. Also, this value can be quantified as ca. 1.56 times by carefully measuring the mass of the SiO_2 layer after both wafers were subject to thermal oxidation.[19]

Figure 4 compares the reflectivity and EQE dependences on wavelengths of *mc*-Si, B*mc*-Si, and P*mc*-Si solar cells. Figure 4a gives the reflectivity dependence on wavelength of three types of wafers before and after SiN_x coating (as a comparison, the curves of *sc*-Si are also included). The average reflectivity $\overline{R}$ (350–1050 nm) of *mc*-Si, B*mc*-Si, P*mc*-Si, and *sc*-Si wafers before/after SiN_x coating is about 24.46%/9.63%, 6.53%/4.55%, 13.75%/3.59%, and12.50%/3.32%, respectively. Note, after metallization the average reflectivity of cells has an additional increase of ca. 2%. Before SiN_x coating, B*mc*-Si could trap more light than others due to a deeply density-graded nanostructure,[36] but its superiority was surpassed by both P*mc*-Si and *sc*-Si after SiN_x coating. An apparent reason is that the SiN_x is too thick and not conformal to the nanopore structure of B*mc*-Si.

For silicon solar cells, it is a common requirement to have relatively low reflection at the spectra of interest (i.e., from 400 to 1000 nm). Unfortunately, the reflections of SiN_x-coated *mc*-Si are much fluctuant in this range, and its near-zero reflections are only at very narrow zone near 650 nm, which is limited by the certain thickness of the SiN_x layer (ca. 90 nm) designed as a quarter-wavelength antireflection coating based on interference effect.[17] In contrast, the nanopyramid texture endows P*mc*-Si with an additional confinement to the light over a broad range of spectra, thus its near-zero reflections are quite constant in a range from 500–800 nm. This can be explained in that the nanopyramid texture, as a density-graded layer, can suppress *R* exponentially with grade depth.[12] Consequently, the P*mc*-Si has very similar optical properties as *sc*-Si, i.e., both reflection curves are very close, but there is more expectation with respect to its electrical properties.

Figure 4b compares the EQEs of *mc*-Si, B*mc*-Si, and P*mc*-Si solar cells. First, the poor spectral response is observed in B*mc*-Si solar cell (similar to that of the nanoporous *mc*-Si cell in Shi et al.[30]), i.e., EQE is only 8% at 400 nm, 70% at 600 nm and 58% at 1000 nm, which are well below those corresponding values of 66%, 93%, and 77% for *mc*-Si cells, repectively. Obviously, the B*mc*-Si solar cell is over-nanostructured with high surface area, where most of photogenerated *e-h* pairs are recombined, although it can trap more light than others. Oh et al. have reported an improved blue quantum efficiency by decreasing the nanopore depth.[19] In our case, P*mc*-Si solar cell

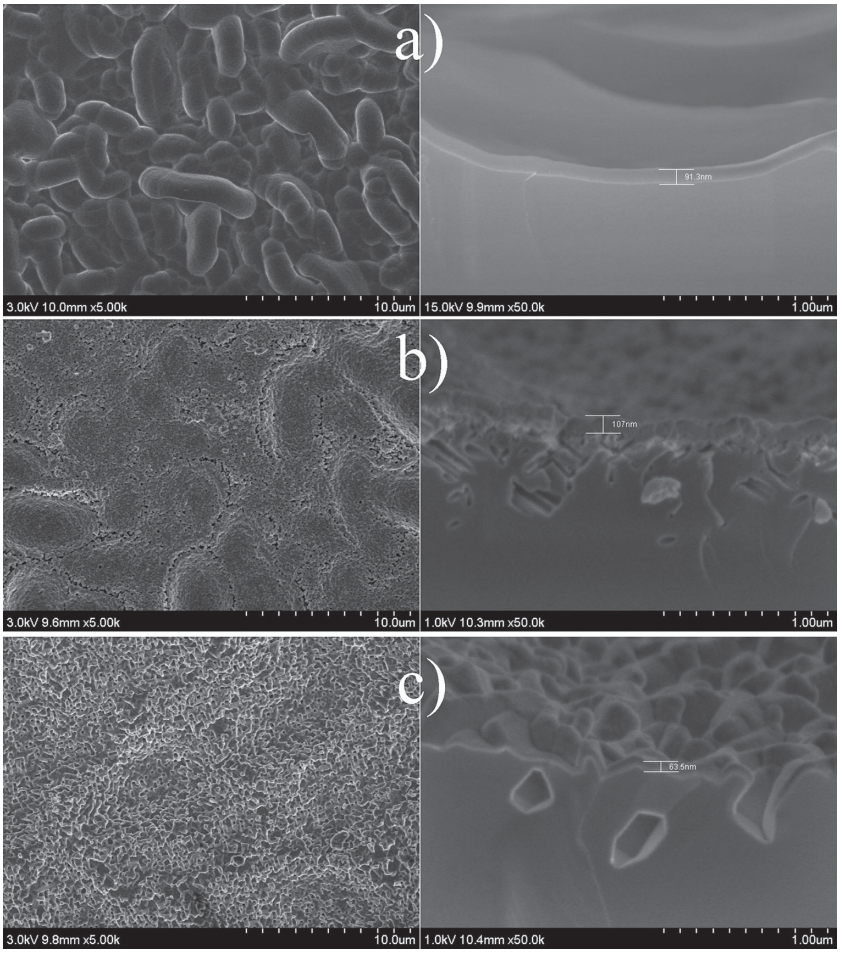

Figure 3. Surface (left) and cross-section (right) SEM images of SiN_x-coated wafers: a) *mc*-Si, where the SiN_x/Si interface is clear and dense; b) B*mc*-Si, where SiN_x piled on the surface, and, c) P*mc*-Si, where SiN_x is almost conformal to the pseudo-pyramid texture.

shows a great EQE improvement compared to the B*mc*-Si one by decreasing the depth of nanostructure. More interestingly, under an alkaline etching step its nanostructure is no longer pore shape but pseudo-pyramid shape, leading to an improved spectral response among wavelengths 300–600 nm compared to *mc*-Si.

Figure 5 is the phosphorus concentration dependence on depth of *mc*-Si, B*mc*-Si, and P*mc*-Si samples, showing a non-linear curve of doping distribution inside the emitter zone (0–500 nm). The B*mc*-Si solar cells have very high concentration (>10^{19} cm^{-3}) near a thickness of 20 nm, which is larger than that of *mc*-Si and P*mc*-Si (>$10^{18}$$cm^{-3}$). The surface concentrations of the three samples are consistent with the measured surface sheet resistances, as marked in the figure. For doping concentrations higher than 10^{18} cm^{-3} in silicon, Auger recombination will cause low lifetime and high surface recombination velocities in the emitter.[19] The insert images of Figure 5 indicate that the openings of the pseudo-pyramid nanostructure are much larger than those of the nanopores, thus providing the benefit of a modified distribution of phosphorus doping and depressing the stonger Auger recombination in the surface.

Figure 6 schematically illustrates a cross-section of a p-n^+ junction and the doping profiles on the textured *mc*-Si wafers. For *mc*-Si solar cells, the concentration of *p*-type silicon wafer (N_p) is ca. 10^{16} cm^{-3}, and the average *n*-type doping (N_n) is ca. 10^{18} cm^{-3} with the phosphorus doping depth being ca. 500 nm. Roughly, we can calculate the width of depletion zone for a p-n^+ junction based on the following equation:[37]

$$W = \sqrt{\frac{2\varepsilon_0\varepsilon_r}{q}\left(\frac{N_p + N_n}{N_p \times N_n}\right)V_{bi}}\,;\, V_{bi} = \frac{kT}{q}\ln\left(\frac{N_p \times N_n}{n_i^2}\right) \quad (1)$$

Here, W is the width of depletion zone, which almost totally locates in the *p*-type side in a p-n^+ junction; ε_0 is the permittivity of a vacuum, and ε_r (ca. 11.9) is the relative permittivity of silicon; N_i (ca. 10^{10} cm^{-3}) is the intrinsic carrier concentration of silicon; q is the electron charge; V_{bi} is the built-in voltage of the p-n junction; k is Boltzmann's constant, and T (ca. 300 K) is temperature in Kelvin.

Therefore, the calculated W is ca. 1.1 µm, which is about double the depth of the n^+ zone. However, the nanoholes (ca. 350 nm in depth) of B*mc*-Si wafer penetrating two-thirds into the n^+ doping area, will certainly distort the depletion zone profile of p-n junction as well as V_{bi}. Besides, the deep nanostructure will elongate the collection path of the photogenerated electrons to the front finger contacts. Neverthless, one can image that the thin emitter in planar solar cells will be very sensitive to the nanostructure. Therefore, P*mc*-Si wafers of shallow pyramid texture (ca. 150 nm in depth) are expected to overcome those problems to have better cell performance than B*mc*-Si cells.

4. 18.45%-Efficient *mc*-Si Solar Cells with Nanoscale Pseudo-Pyramid Texture

Figure 7 presents the *I*–*V* curves of *mc*-Si, B*mc*-Si, and P*mc*-Si solar cells. The main characteristics are listed in **Table 2**. Commonly, a silicon solar cell should have higher power conversion ability when more light is absorbed inside. However, it seems that the enhancement of efficiency is not always synchronous with the increase of light absorption, especially when the nanostructure is introduced on the surface of cell. The efficiency of P*mc*-Si solar cell ($\overline{R}$, ca. 6%) reaches 18.45%, i.e., the I_{sc} has an increase of ca. 300 mA but V_{oc} has a decrease of ca. 2 mV to the 17.89%-efficient *mc*-Si ($\overline{R}$, ca. 12%). To our knowledge, 18.45% is the highest reported efficiency based on the MCCE technique. The results indicate that the P*mc*-Si cell has enhanced light absorption, especially in the blue and green spectra.

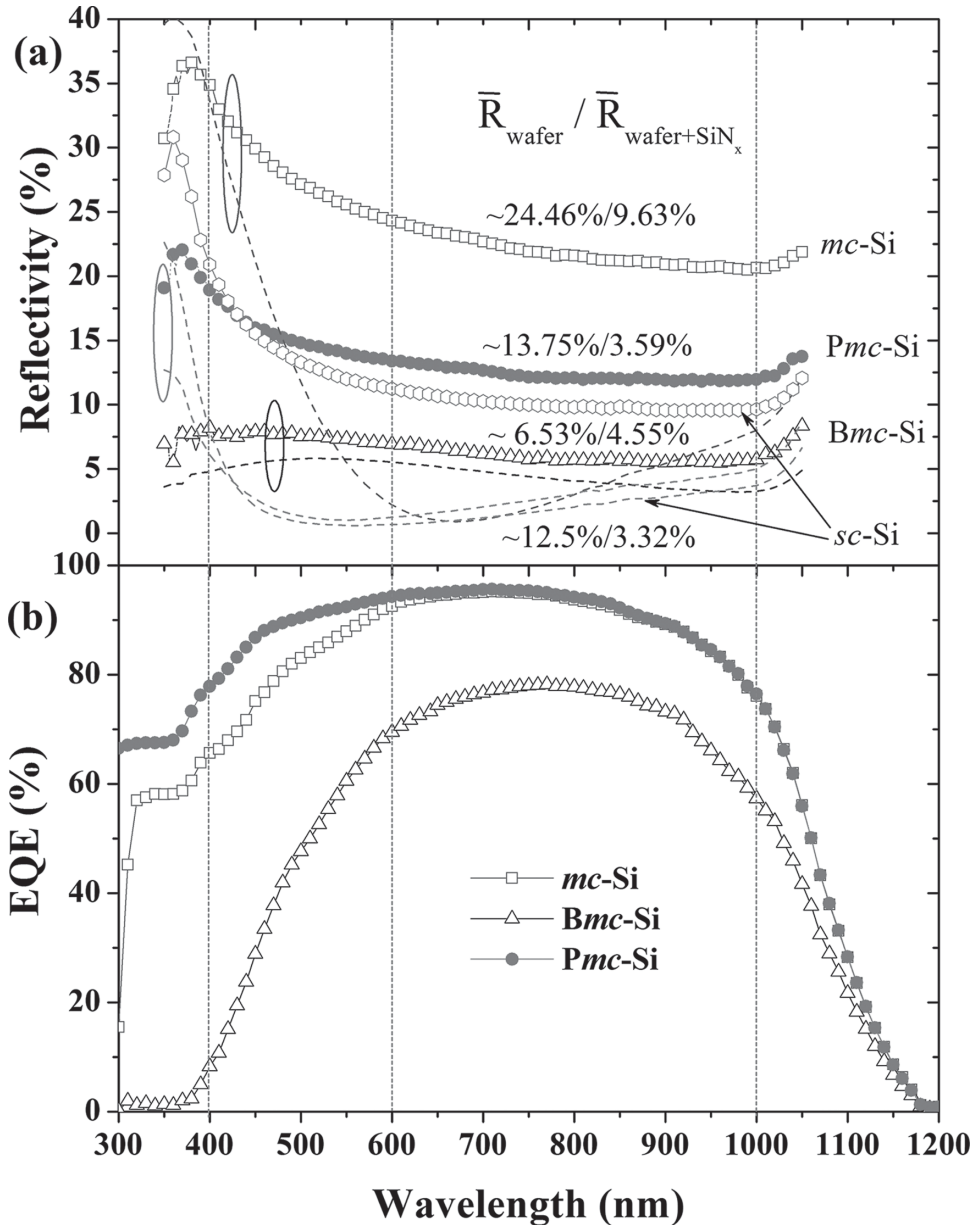

Figure 4. a) Reflectivity of three mc-Si wafers and one sc-Si wafer before and after SiN_x coating, and, b) EQE of three mc-Si cells. Dash lines are guides to the eye at three important wavelengths at 400, 600, and 1000 nm. SiN_x-coated P*mc*-Si wafer has similar reflection as *sc*-Si, showing the best blue spectral response among three *mc*-Si cells. The *sc*-Si wafer has a pyramid-texture after standard alkali etching while the *mc*-Si has an oval-pit texture after standard acidic etching.

The bad performance of 16.51%-efficient B*mc*-Si solar cell ($\overline{R}$, 6.5%) indicated that the highly nanostructured surface has strong impacts on the electronic properties, being mainly deteriorated by over-doping/Auger recombination and incomplete passivation of SiN_x. Besides, some Ag nanoparticles still reside deeply in the nanostructured B*mc*-Si wafer even after a careful cleaning process, but under the detection limit for P*mc*-Si wafers (see Supporting Information S4). Those liabilities in B*mc*-Si are embodied in the very low lifetime, poor EQE, and low efficiency.

Finally, we will take a simple calculation to find out how far the η can be pushed through enhanced light absorption for regular solar cells. In the equation for the power conversion efficiency of solar cells, $\eta = \frac{J_{sc} \times V_{oc}}{P_{in}} \times FF$, where FF and P_{in} is filling factor and 1 Sun power (ca. 100 mW cm^{-2}), respectively. Similar to definition of external and internal quantum efficiency, we can define external and internal power conversion efficiency η_{ex} and η_{in}, and $\eta_{in} = \eta_{ex}/(1 - \overline{R})$, where $\overline{R}$ is reflectivity after metallization. For an η_{ex} = 17.5% *mc*-Si solar cell with typical $\overline{R}$ = 12%, η_{in} = 17.5%/0.88 = 19.89%. Ideally, for a P*mc*-Si solar cells with typical $\overline{R}$ = 6%, which is 6% lower than that of *mc*-Si solar cell, the η can be improved by 18.89% × 6% ≈ 1.13%. In the same batch, our best P*mc*-Si cell is about ca. 0.56% higher than that of the best *mc*-Si solar cell. It also

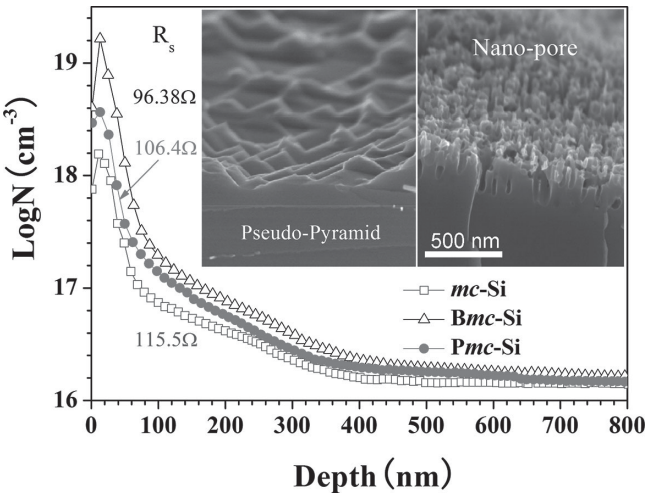

Figure 5. Phosphorus doping distribution of *mc*-Si, B*mc*-Si, and P*mc*-Si wafers. Insert: Cross-sectional SEM images of B*mc*-Si (right) and P*mc*-Si (left) wafers. The sheet resistances of three samples are labelled to the curves. The nanopore textured wafer has over-doped surface, thus leading to strong recombination.

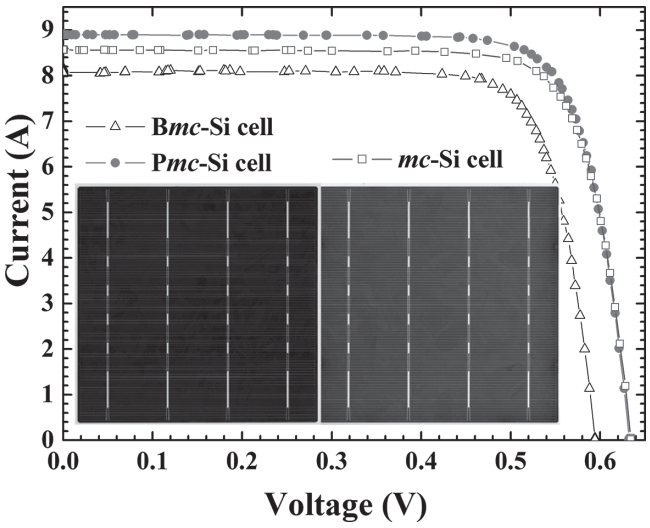

Figure 7. *I–V* curves of mc-Si, Bmc-Si, and Pmc-Si solar cells. Insert: photos of *mc*-Si and P*mc*-Si solar cells. The measurement area is 15.6 cm × 15.6 cm, and the corresponding current density of P*mc*-Si is 36.7 mA cm^{-2} under AM 1.5G illumination. The efficiencies are measured with an IV measurement system (Berger PSL-SCD, Germany) calibrated with the standard cells of Fraunhofer Institute for Solar Energy Systems, Germany.

implies that some part of the enhanced light absorption fails yet for the photoelectric conversion. To further improve η, a more effective passivation technique must be explored for the P*mc*-Si solar cells in the future.[29]

With intensive research and development from institutes and industries all over the world in recent decades, it has become more and more difficult to find a revolutionary technique, which is suitable (requiring low cost and high efficiency) for the mass production of mc-Si solar cells.

Thousands of P*mc*-Si solar cells with an average efficiency over 18% have been fabricated in a standard production line, and the figure of merit is ca. \$0.0084 W^{-1} better than that of *mc*-Si one (see Supporting Information S5). Such results are very tantalizing for the whole photovoltaic community. The strategies taking to improve efficiency on industrial scale can be concluded as: i) a uniform pre-texturised surface will benefit the deposition of Ag nanoparticles homogeneously, and results in an orientation-independent nanostructure; ii) a tradeoff between optical gain and recombination loss must be considered to achieve high J_{sc} while keep normal V_{oc}; iii) a unique pyramidal structure not only can bear possible damage during the following processing steps including diffusion, PSG etching, and PECVD, but also is prone to unremoved Ag residuals; iv) for industrial production, it is important that our nanotexture technique can be easily integrated into current product lines while remaining cost-effective. We believe the technique of MCCE plus post-alkaline etching has staked out a solid step towards mass production, and it has a great potential to become a standard process for producing highly efficient *mc*-Si solar cells in the future.

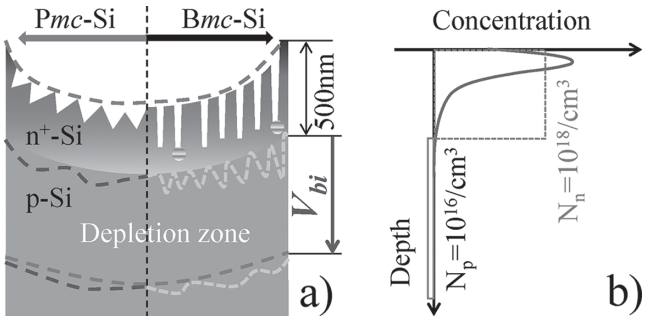

Figure 6. Schematic illustration of: a) p-n^+ junction, and, b) doping profiles on the textured *mc*-Si wafers. The deep nanostructure in B*mc*-Si wafer penetrating into almost two-third of n^+ zone strongly distorts the profile of depletion zone as well as V_{bi}, also causes difficulties in removing Ag nanoparticles and collecting electrons to the top finger contacts; the shallow pyramid texture in P*mc*-Si wafer can greatly ease those influences.

5. Conclusions

In summary, contrary to common belief, a nanoscale pseudo-pyramid texture, which usually cannot be achieved via regular methods such as acidic and alkali etching, or plasma etching, has been uniformly incorporated into the multi-crystalline silicon solar cells by using metal-catalyzed chemical etching and alkaline etching methods. The formation mechanism of this unique nanoscale pseudo-pyramid texture in *mc*-Si wafer has been discussed. We believe that the unique pyramidal structure ensures the multi-crystalline silicon surface is covered by the

Table 2. Main characteristics of *mc*-Si solar cells with different textures.

Sample	V_{oc} [V]	I_{sc} [A]	*FF* [%]	τ [μs]	η [%]
mc-Si	0.636	8.625	79.35	15.92	17.89
B*mc*-Si	0.615	8.379	77.95	1.53	16.51
P*mc*-Si	0.634	8.928	79.31	10.48	18.45

most close-packed {111} crystal surface, thus benefiting not only its light-trapping but also its electron-transporting abilities. Consequently, an 18.45%-efficient P*mc*-Si solar cell has been fabricated on an industrial production line, which has a ca. 300 mA cell^{-1} increase in the short-circuit current density but only a slight decrease in open-circuit voltage compared to the regular *mc*-Si solar cell. The P*mc*-Si solar cells have showed synchronous improvements of light absorption and electric properties due to the enhancement of light absorption and the acceptable passivation quality with PECVD-SiN_x coating. Further elevations of the efficiency are expected by optimizing both micrometer- and nanotextures, and exploring more effective passivation techniques.

6. Experimental Section

Sample Fabrication: Multi-crystalline Si wafers (15.6 cm × 15.6 cm × 0.18 cm, p-type, specific resistance $\rho = 1$–$3\ \Omega$ cm, GCL company, China) was used for this work. Usually, a standard process for producing *mc*-Si solar cells consists of four main steps: acid etching to obtain a micrometer-textured surface, phosphorus diffusion to form *p-n* junction emitters, PECVD to deposit the SiN_x antireflection/passivation layer, and screen printing to metalize top/bottom electrodes. To obtain B*mc*-Si and P*mc*-Si solar cells, a novel nanotexture process was incorporated into the standard process of *mc*-Si solar cell after the normal acid etching. First, Ag nanoparticles were deposited on the micrometer-textured surface of *mc*-Si wafer by dipping the wafer in $AgNO_3/HF/H_2O$ mixture solution ($AgNO_3$ in 0.001–0.2 mol L^{-1}, HF in 0.01–0.05 mol L^{-1}) for 10 s. Second, the samples were etched in $HF/H_2O_2/H_2O$ (HF at 1–5 mol L^{-1}, H_2O_2 at 1–2 mol L^{-1}) mixture solution at room temperature for 5 min. Due to the strong catalytic action, the Ag nanoparticles sunk into the substrate rapidly, thus leaving numbers of nanopores on the surface; at this stage, the wafer was eventually dipped in a diluted HNO_3 solution for 3 min in order to remove Ag, and labeled as B*mc*-Si. Third, the B*mc*-Si wafers were etched in NaOH/H_2O solution (NaOH in 0.005–0.2 mol L^{-1}, 80 °C) for 120 s to convert above the nanopores into pseudo-pyramids, labeled as P*mc*-Si. Finally, a standard SC2 clean ($HCl/H_2O_2/H_2O$ = 1:1:6, 80 °C, 15 min) was applied to reduce or completely remove residual silver particles.

Sample Characterization: In order to compare the optical and electronic properties, three types of cell, that is, *mc*-Si, B*mc*-Si, and P*mc*-Si, were fabricated in the same batch on a standard product line. The microstructure, reflection, external quantum efficiency (EQE), doping concentration, surface sheet resistance, lifetime of minority carrier, and *I–V* curves of cells were measured by SEM (Hitachi, S4800, Japan), TEM (FEI Tecnai G2F20S-Twin,USA), reflectometetry (Radiation Technology D8, China), PV measurements (QEX7, USA), ECV Pro (Nanometrics, UK), 4 Probe sheet resistance tester (Napson RT-70V, Japan), IV measurement system (Berger PSL-SCD, Germany), and WT2000 (Semilab WT2000, Hungary).

Supporting Information

Supporting Information is available from the Wiley Online Library or from the author.

Acknowledgements

This work was supported by the Natural Science Foundation of Jiangsu province under grant no. BK2012622, by the Prospective Project of Industry-University-Research Institution of Jiangsu province under grant no. BY2013030–01, and by the Priority Academic Program Development of Jiangsu Higher Education Institutions (PAPD). The authors would like to thank Prof. Liang Li for many helpful discussions. The efficiency value provided in the last paragraph of the Introduction Section was corrected on November 12, 2014.

Received: May 16, 2014
Revised: June 17, 2014
Published online: August 22, 2014

[1] E. Lee, H. Lee, J. Choi, D. Oh, J. Shim, K. Cho, J. Kim, S. Lee, B. Hallam, S. R. Wenham, H. Lee, *Solar Energy Mater. Solar Cells* **2011**, *95*, 3592–3595.
[2] S. J. Eisele, T. C. Röder, J. R. Köhler, J. H. Werner, *Appl. Phys. Lett.* **2009**, *95*, 133501.
[3] S. Gatz, K. Bothe, J. Müller, T. Dullweber, R. Brendel, *Energy Proc.* **2011**, *8*, 318.
[4] N. Bateman, P. Sullivan, C. Reichel, J. Benick, M. Hermle, *Energy Proc.* **2011**, *8*, 509.
[5] W. W. Yin, X. S. Wang, F. Zhang, L. J. Zhang, *IEEE J. Photovolt.* **2013**, *3*, 697.
[6] H. Seidel, L. Csepregi, A. Heuberger, H. Baumgärtel, *J. Electrochem. Soc.* **1990**, *137*, 3626.
[7] P. Panek, M. Lipinski, J. Dutkiewicz, *J. Mater. Sci.* **2005**, *40*, 1459.
[8] T. H. Her, R. J. Finlay, C. Wu, S. Deliwala, E. Mazur, *Appl. Phys. Lett.* **1998**, *73*, 1673.
[9] F. Toor, H. M. Branz, M. R. Page, K. M. Jones, H. C. Yuan, *Appl. Phys. Lett.* **2011**, *99*, 103501.
[10] J. Yoo, G. Yu, J. Yi, *Sol. Energy Mater. Sol. Cells* **2011**, *95*, 2.
[11] M. Halbwax, T. Sarnet, Ph. Delaporte, M. Sentis, H. Etienne, F. Torregrosa, V. Vervisch, I. Perichaud, S. Martinuzzi, *Thin Solid Films* **2008**, *516*, 6791.
[12] H. C. Yuan, V. E. Yost, M. R. Page, P. Stradins, D. L. Meier, H. M. Branz, *Appl. Phys. Lett.* **2009**, *95*, 123501.
[13] C. H. Crouch, J. E. Carey, J. M. Warrender, M. J. Aziz, E. Mazur, *Appl. Phys. Lett.* **2004**, *84*, 1850.
[14] P. Choulat, G. Agostinelli, D. Dehertoghe, G. Beaucarne, *Proc. 22nd Eur. Photovoltaic Solar Energy Conf. Milan, Italy* **2007**.
[15] a) H. Jansen, M. de Boer, R. Legtenberg, M. Elwenspoek, *J. Micromech. Microeng.* **1995**, *5*, 115; b) D. S. Ruby, S. H. Zaidi, S. Narayanan, B. M. Damiani, A. Rohatgi, *Sol. Energy Mater. Sol. Cells* **2002**, *74*, 133.
[16] S. Koynov, M. S. Brandt, M. Stutzmann, *Phys. Status Solidi (RRL)* **2007**, *1*, R53.
[17] S. Koynov, M. S. Brandt, M. Stutzmann, *Appl. Phys. Lett.* **2006**, *88*, 203107.
[18] S. Bastide, N. Quang, R. Monna, C. Lévy-Clément, *Phys. Status Solidi C* **2009**, *6*, 1536.
[19] J. Oh, H. C. Yuan, H. M. Branz, *Nat. Nanotechnol.* **2012**, *7*, 743.
[20] M. D. Kelzenberg, S. W. Boettcher, J. A. Petykiewicz, D. B. Turner-Evans, M. C. Putnam, E. L. Warren, J. M. Spurgeon, R. M. Briggs, N. S. Lewis, H. A. Atwater, *Nat. Mater.* **2010**, *9*, 239.
[21] K. Fukui, K. Okada, Y. Inomata, H. Takahashi, S. Fujii, Y. Fukawa, K. Shirasawa, *Solar Energy Mater. Solar Cells* **1997**, *48*, 219.
[22] P. Repo, J. Benick, V. Vähänissi, J. Schön, G. von Gastrow, B. Steinhauser, M. C. Schubert, M. Hermle, H. Savin, *Energy Proc.* **2013**, *38*, 866.
[23] W. C. Wang, C. W. Lin, H. J. Chen, C. W. Chang, J. J. Huang, M. J. Yang, B. Tjahjono, J. J. Huang, W. C. Hsu, M. J. Chen, *ACS Appl. Mater. Interfaces* **2013**, *5*, 9752.
[24] K. Tsujino, M. Matsumura, Y. Nishimoto, *Sol. Energy Mater. Sol. Cells* **2006**, *90*, 100.
[25] Z. P. Huang, G. Nadine, P. Werner, J. de Boor, U. Gösele, *Adv. Mater.* **2011**, *23*, 285.
[26] K. Q. Peng, H. Fang, J. J. Hu, Y. Wu, J. Zhu, Y. J. Yan, S. T. Lee, *Chem. – Eur. J.* **2006**, *12*, 7942.

[27] C. Chartier, S. Bastide, C. Levy-Clement, *Electrochim. Acta* **2008**, *53*, 5509.
[28] M. Algasinger, M. Bernt, S. Koynov, M. Stutzmann, *J. Appl. Phys.* **2014**, *115*, 164308.
[29] M. Algasinger, J. Paye, F. Werner, J. Schmidt, M. S. Brandt, M. Stutzmann, S. Koynov, *Adv. Energy Mater.* **2013**, *3*, 1068.
[30] J. Shi, F. Xu, P. Zhou, J. Yang, Z. Yang, D. Chen, Y. Yin, D. Chen, Z. Ma, *Solid-State Electron.* **2013**, *85*, 23.
[31] U. Gangopadhyay, S. K. Dhungel, K. Kim, U. Manna, P. K. Basu, H. J. Kim, B. Karunagaran, K. S. Lee, J. S. Yoo, J. Yi, *Semicond. Sci. Technol.* **2005**, *20*, 938.
[32] K. Peng, A. Lu, R. Zhang, S. T. Lee, *Adv. Funct. Mater.* **2008**, *18*, 3026.
[33] V. Lehmann, *J. Electrochem. Soc.* **1993**, *140*, 2836.
[34] K. Tsujino, M. Matsumura, *Adv. Mater.* **2005**, *17*, 1045.
[35] Z. P. Huang, T. Shimizu, S. Senz, Z. Zhang, N. Geyer, U. Gösele, *J. Phys. Chem. C* **2010**, *114*, 10683.
[36] H. M. Branz, V. E. Yost, S. Ward, K. M. Jones, B. To, P. Stradins, *Appl. Phys. Lett.* **2008**, *94*, 231121.
[37] M. S. Simon, M. K. Lee, *Semiconductor Devices: Physics and Technology*, John Wiley & Sons Ltd., USA **2012**.